http://dx.doi.org/10.1590/1981-86372022005320210090

| ORIGINAL

Implant site preparation-related bone microdamage: An alternative ex vivo analysis of drilling speed protocols

Microdanos ósseos gerados na preparação do sítio de instalação de implantes: uma alternativa para análise ex vivo de diferentes protocolos de velocidade de perfuração

Isabella de Almeida **FRANCISQUINI**[1] 0000-0001-9906-2145

Gustavo Davi **RABELO**[2] 0000-0001-9511-5078

Neuza Maria Souza Picorelli **ASSIS**[1] 0000-0002-8612-5044

Bruno Salles **SOTTO-MAIOR**[3] 0000-0002-9462-0299

Pedro Henrique Justino Oliveira **LIMIRIO**[4] 0000-0002-0089-3772

Karina Lopes **DEVITO**[1] 0000-0001-5037-5466

ABSTRACT

Objective: The aim of this study was to evaluate bone microdamage in sites prepared for implant placement by using an ex vivo model with three drilling rotation speeds. **Methods**: Bovine bone ribs were used for the creation of 18 osteotomy sites at different rotation speeds: 1200 rpm, 800 rpm, and 400 rpm. Specimens were stained with xylenol orange and prepared for histological analysis by using fluorescence and polarized light microscopies. Bone microdamage was evaluated by number and based on total bone area, as follows: microfracture density (Fr.D = n/mm^2), microcrack morphology (diffuse or linear), and density (Cr.D = n/mm^2), and presence of bone chips. To complement the analysis, linear microcracks were assessed by using confocal microscopy for three-dimensional visualization. **Results**: Bone microdamage on the osteotomy sites included microcracks, diffuse damages, microfracture, and bone chip formation. There was an association between bone microdamage and cancellous bone (p 0.0016), as well as a positive correlation between Fr.D and Cr.D (p 0.05, r 0.54). BM occurrence was not different between the three rotation speeds. In 3D, the height of the microcrack depth was 60.81 µm. **Conclusion**: Bone microdamage occurs during osteotomy, and the ex vivo model used was effective for the assessment of these biomechanical parameters. In addition, microdamage was not influenced by the drilling rotation speed in this experimental condition.

Indexing terms: Bone and bones. Histology. Osteotomy.

[1] Universidade Federal de Juiz de Fora, Faculdade de Odontologia, Departamento de Clínica Odontológica. Juiz de Fora, MG, Brasil.
[2] Universidade Federal de Santa Catarina, Departamento de Odontologia. Rua Delfino Conti, 1240, 88040-900, Trindade, Florianópolis, SC, Brasil. Correspondence to: GD Rabelo. E-mail: <drgustavorabelo@yahoo.com.br>.
[3] Universidade Federal de Juiz de Fora, Faculdade de Odontologia, Departamento de Odontologia Restauradora. Juiz de Fora, MG, Brasil.
[4] Universidade Federal de Uberlândia, Faculdade de Odontologia, Departamento de Odontologia. Uberlândia, MG, Brasil.

How to cite this article

Francisquini IA, Rabelo GD, Assis NMSP, Sotto-Maior BS, Limirio PHJO, Devito KL. Implant site preparation-related bone microdamage: An alternative ex vivo analysis of drilling speed protocols. RGO, Rev Gaúch Odontol. 2022;70:e20220053. http://dx.doi.org/10.1590/1981-86372022005320210090

RESUMO

***Objetivo**: O objetivo desse estudo foi avaliar os microdanos ósseos em locais preparados para a instalação de implantes utilizando um modelo ex vivo acessando três velocidades de rotação de perfuração. **Métodos**: Fragmentos ósseos de costela bovina foram utilizados para a criação de 18 sítios de osteotomia em diferentes velocidades de rotação: 1200 rpm, 800 rpm e 400 rpm. As amostras foram coradas com Alaranjado de Xilenol e preparadas para análise microscópica em fluorescência e luz polarizada. Os microdanos ósseos foram avaliados em número e calibrados com base na área total óssea: densidade de microfraturas (Fr.D = n/mm^2), morfologia (difusa ou linear) e densidade de microtrincas (Cr.D = n / mm^2) e presença de espículas ósseas. Para complementar a análise, microtrincas lineares foram avaliadas por meio de microscopia confocal para visualização tridimensional. **Resultados**: Os microdanos ósseos incluíram microtrincas, danos difusos, microfraturas e formação de espículas. Houve uma associação entre MO e localização em osso esponjoso (p=0,0016), bem como uma correlação positiva entre Fr.D e Cr.D (p=0,05, r = 0,54). A ocorrência de microdanos ósseos não foi diferente entre as três velocidades de rotação utilizadas. Em 3D, a profundidade maior da microfissura atingiu 60,81 µm. **Conclusão**: Microdanos ósseos ocorrem durante a osteotomia e podem ser acessados em um modelo ex vivo na condução de experimentos em biomecânica. Sugere-se que a presença de microdanos não é influenciada pela velocidade de rotação durante a perfuração.*

Termos de indexação: *Osso e ossos. Histologia. Osteotomia.*

INTRODUCTION

Implant placement requires the bone to be perforated through osteotomy, which is necessary for preparation of the implant site. Different surgical drills are sequentially used following distinct steps [1,2]. A drilling protocol to be followed step-by-step is recommended to minimize trauma during osteotomy, thus reducing the potential formation of excessive bone damage [3,4]. In fact, bone damage is predicted along the entire perforation site depending on the osteotomy procedure. Bone microdamage is supposed to be generated by both drilling procedure [5] and implant placement, which may have crucial implications on the initial healing and later remodeling phases [6].

About bone damage, it was reported that generation of microcracks after osteotomy preparation for implant insertion of endosseous implants occurred in an animal model [5]. Among the types of bone microdamage, microcracks draw more attention as they act as targets for bone remodeling, also regulating bone physiology [7-9]. Accumulation of microdamage, including microcracks, affects the biomechanical properties of bone by reducing its resistance [7]. In physiological conditions, especially regarding microcracks [10], this linear damage occurs in compression as it appears as ellipsoidal planes of separation, particularly in interstitial, extra-osteonal, highly mineralized areas within the cortex [11]. Besides the microcracks, other types of bone microdamage (e.g., microfractures and diffuse damage) are expected to occur and are important in the events leading to remodeling, both in cortical and cancellous bone [12,13].

Besides the damage to the bone structure, drilling also produces small bone fragments called bone chips as a result of cutting forces [14]. These bone chips are characterized as micro fragments resulting from the cutting movement of the drill, being usually accompanied by formation of debris. As the depth of the cut increases during osteotomy, chip formation changes from a fragmentary type to a continuous one [15], so both types are expected.

Therefore, damage formation should be expected as the compression load takes place because of the force applied from the circumferential implant to the bone. The question is whether an excessive damage to bone may cause a break in the balance between damage and repair. How much of the microdamage could be avoided during osteotomy and later in the implant placement? It is not known whether the sequence of events in bone healing and remodeling would occur properly in cases where an acceptable amount of bone microdamage formation is exceeded.

To accurately assess the bone microdamage, we believe that an experimental study seems a viable option to assess different osteotomy protocols, depending on different drilling rotation speeds. Although, the evaluation of bone microdamage is possible only through destructive histological techniques [7]. In this way, seems that the use of bovine bone (usually a waste material) could be a good option for biomechanical experiments before going to an in vivo study, also, providing condition to test several damage generation situations. Therefore, the aim of this study was to perform an ex vivo experimental study on the formation of bone microdamage occurring during osteotomy in sites prepared for implant placement, while also evaluating the influence of different rotation speeds on microdamage generation.

METHODS

Experimental procedures

Six bone fragments of 90 x 40 mm were extracted from two fresh ribs (30 cm each), in one skeletally mature bovine animal were used in this study. Animals were not used exclusively for this study and the bones were collected as it was disposable as waste material. Bovine bone was selected due to its similarities with human mandibular bone, in terms of density and cortical/cancellous bone relation [3]. Bone fragments were obtained through manual sawing (figure 1) and had all the soft tissue removed to ensure that residue did not interfere with the mechanical properties. The fragments were then segmented into 18 bone blocks (~30 mm x 40 mm), each one containing one osteotomy site. Cortical thickness of the bone blocks varied between 1.8 and 2.3 mm.

For drilling, the fragments were randomly divided according to the drilling speed groups division and were positioned into a fixed device to perform the perforations into the bone (figure 1A). Then, the blocks removed from

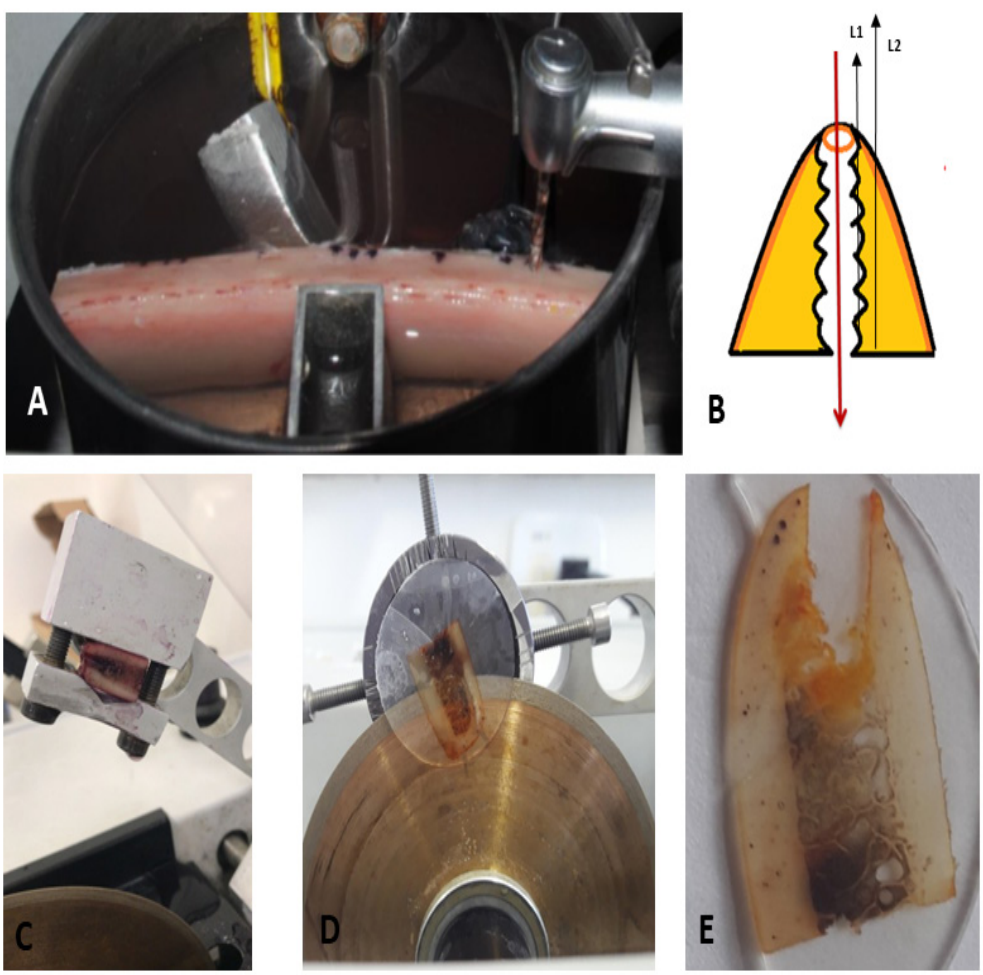

Figure 1. Osteotomy procedure and histological slides preparation. A) Bone fragment fixed to produce osteotomy perforations. B) Schematic representation of the cutting orientation, in order to provide two slides for analysis: L1 and L2. The downward arrow represents the axis of the perforation and the red circle stands for the site chosen for the perforation, meaning the entrance of the drill. C) Cutting of the blocks before embedding. D) Cutting the MMA embedded block at the precision cutter for histological slides obtention. E). Slice obtained for histological analysis. It is possible to macroscopically identify the cortical and cancellous part, and the osteotomy site in the middle.

fragments were separated according the 3 groups drilling speed: 1200 rpm (Group 12, n= 6), 800 rpm (Group 8, n= 6), and 400 rpm (Group 4, n= 6). The site chosen for osteotomy was the surface of the cortex at the top of the bone fragment. The width direction was from the cortex to the cancellous, at the long axis of the bone. Osteotomy was conducted according to the manufacturer's instructions for drilling: a pilot drill was used to 10 mm depth, followed by 2- and 3-mm twist drills to 13 mm of depth (SIN Implant System, São Paulo, Brazil). The total drilling sequence was done with the use of a 20:1 reduction handpiece (W&H, Dentalwerk, Bürmoos, Austria), under continuous irrigation (saline solution with a 100 mL/min flow). The handpiece used was linked to electrical-motor equipment with digital control of the rotation, irrigation, and torque (DForce1000, DentFlex, São Paulo, Brazil). The perforations were performed manually, by only one experienced operator, with a load of 2 kg [16] at room temperature (24ºC). The osteotomy perforation entrance site was the cortical area at the upper part of the bone block (cortical external surface (figure 1B).

Bone microdamage evaluation through different microscopies

The blocks were first fixed in a buffered formalin solution for one month and stored. After that, they were immersed in absolute alcohol (99.7%) for one week. The bone blocks were bulk-stained in xylenol orange 5 Mm (Sigma-Aldrich/ Merck, Germany) for 7 days [17]. Each block was sectioned in the middle (long-axis orientation), using the perforation hole as a guide for the sectioning process (figure 1C). A diamond disk coupled in a precision cutter (ISOMET 1000, Buehler, United States of America) was used. Half of the block was dehydrated and embedded in methyl methacrylate (MMA). Two slides were obtained per block: L1) including the perforation site; and L2) adjacent to the perforation (0.4 mm distance L1 from L2, figure 1B). Slides were obtained using an ISOMET 1000 precision cutter (Buehler, United States) with a 15.2 cm x 0.3 mm thick diamond disk at a speed of 350 rpm (figure 1D). The polishing powders were used in a sequence of 80, 220, 320 and 400 grams to reduce the thickness of the slide. Subsequently, they were polished with a sequence of materials, such as: silicon carbide powder, a paste polishing agent containing aluminum oxide, and then undergoing manual washing in tap water. A total of 32 slides proceeded to analysis, with 4 slides being lost during the cutting and polishing procedures.

The slides (~100 µm, figure 1E) were used for bone damage assessment using microscopy evaluation under fluorescent light, with confirmation of the depth of the microdamage in polarized light [17]. The samples were completely evaluated, consisting of both cortical and cancellous parts. Images were obtained for all microdamage and chip formation, using the original magnification of 10X (AXIOPHOT HB 50 ZEISS Microscope, Oberkochen, Germany, coupled to an AxioCam ICc3 camera CCD Basic Resolution: 2080 x 1540 = 3.3 Megapixels, ZEISS, Oberkochen, Germany). Bone microdamage was considered as: a) cortical or cancellous microfractures (a fracture was defined as the separation of two independent fragments, with their surface stained yellow to orange and with a shiny halo under fluorescent light) (figure 2A and 2B), b) microcracks, defined by their linear morphology (sharp edges, depth in field with stained walls, smaller than vessels and greater than canaliculi [7] (figure 2C), c) diffuse damage (a cluster of submicroscopic short fissures and cracks, identifiable by diffuse fluorescent staining in a given area, with these micro linear damages forming a cross-hatch format, figure 2E), both confirmed through their depth under polarized light (figure 2D and 2F), d) bone chips, defined as micro bone particles produced during the osteotomy (figure 2G and 2H), characterized by smaller size fragments, usually forming a cluster, with a shiny halo surrounding all of the particles under fluorescent light.

Bone damage was evaluated considering the total bone area (B.Ar), which was measured in the same slides using a stereoscopic magnifying glass (1x, Discovery .V8, Stereo, Zeiss, Oberkochen, Germany). Cancellous or cortical microfractures were analyzed by their number and location, calculating density (Fr.D) as the total number of fractures divided by the total amount of bone (F/B.Ar; n/mm^2). For the other microdamage evaluation, linear microcrack density (Cr.D) was expressed per unit of bone area (Cr.n/B.Ar; n/mm^2). Diffuse damage was counted in total number. In addition, all microdamage was evaluated according to the following criteria: a) location, whether they were present in the cortical or the cancellous part; b) type of microdamage present, whether it was linear (microcrack) or diffuse damage; c) the size

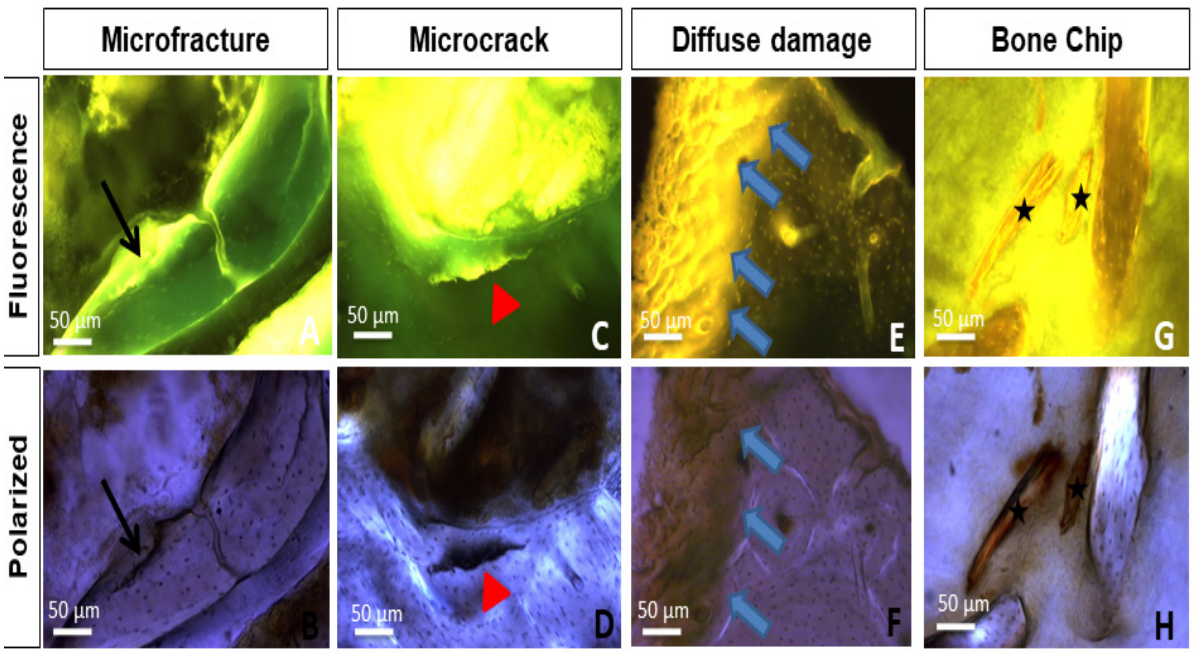

Figure 2. Bone damage representation, all identified in fluorescence microcopy (superior figures A, C, E and G) and confirmed in polarized light microscopy (inferior figures B, D, F and H). Micro-fracture (A and B, black arrow). Microcrack (C and D, red arrow head). Diffuse-damage (E and F, all area pointed by blue arrows). Bone chips (G and H, black asterisk).

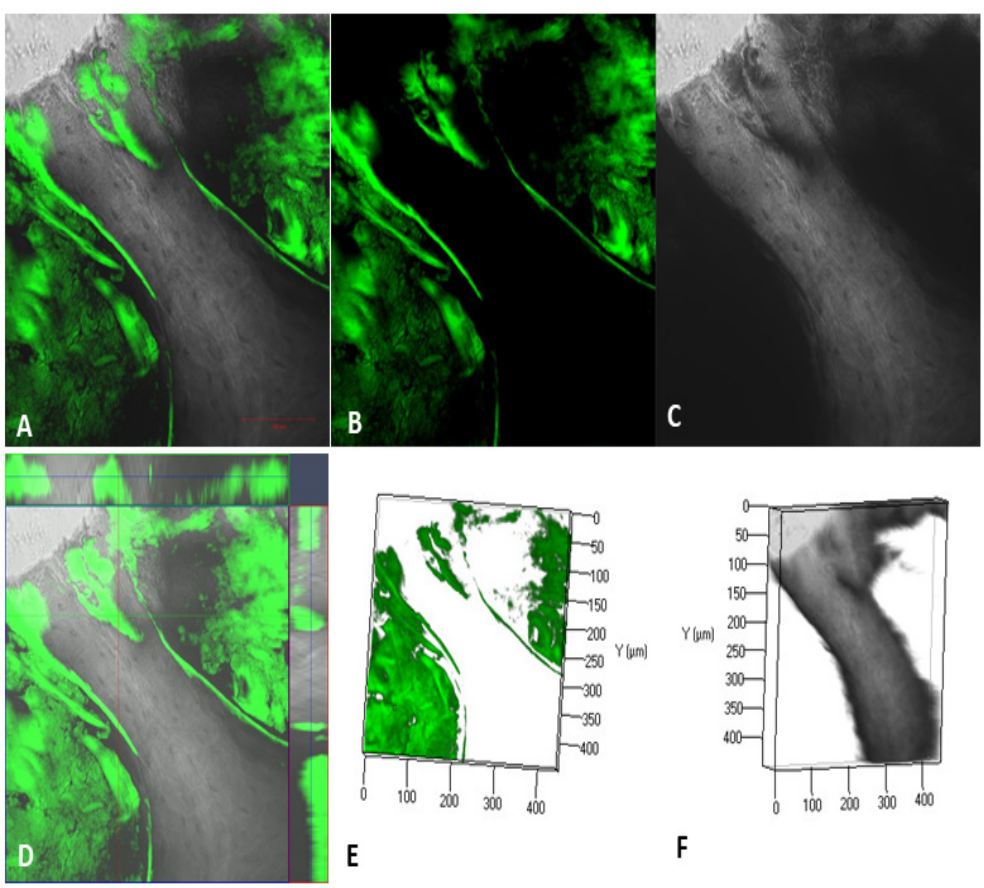

Figure 3. Linear microcrack identified by Confocal Microscopy. Fluorescence identification (B) confirmed by contrast phase (C), analyzed together (A). D) Coronal and Sagittal plane visualization. E and F) Tridimensional reconstruction of the stack formed by the whole microcrack extension analyzed.

of the damage, as the length for the linear microcracks – following the path of the crack (Cr.Le, µm). For bone chip (BC) evaluation, a proportional measurement was performed by scoring (S): 0) no presence of bone chips; 1) presence of a low number of particles/fragments; 2) presence of an average amount of particles; 3) presence of a high number of particles with a shiny bright along the whole cluster of the fragments. For this stated purpose, all bone chips and their forming clusters were identified and then captured in separate images, with the score given by the number of images.

For a better understanding of linear damage morphology, aiming for a qualitative evaluation and improved illustration, two slides were used to assess the three-dimensional structure of the linear microcracks, thus attempting to observe them through their total depth. For this purpose, a confocal microscopy analysis was performed, using the 458 nm argon laser with an emission spectrum between 521-628nm (LSM 510 Meta, Zeiss, Oberkochen, Germany). A stack was created from the bottom to the top of the microdamage for each linear microcrack evidenced in the two histological sections. Both fluorescent and contrast filters were used, and a three-dimensional (3D) image was obtained for each microcrack evidenced separately (figure 3A-F). Another 3D evaluation was performed, obtained from a 2D histological image. A randomly chosen linear microcrack was used (Group 2). The polarized image was insert in ImageJ (Version 1.48, Wayne Rasband, National Institutes of Health, USA), transformed to 8 bits and processed with the tool of contrast enhancement (to normalize and equalize the histogram). The plugin 3D was selected to create an "Interactive 3D Surface Plot" (Grid size of 256, Smoothing of 5.5, and on "Filled" type to visualize on Spectrum LUT, figure 4).

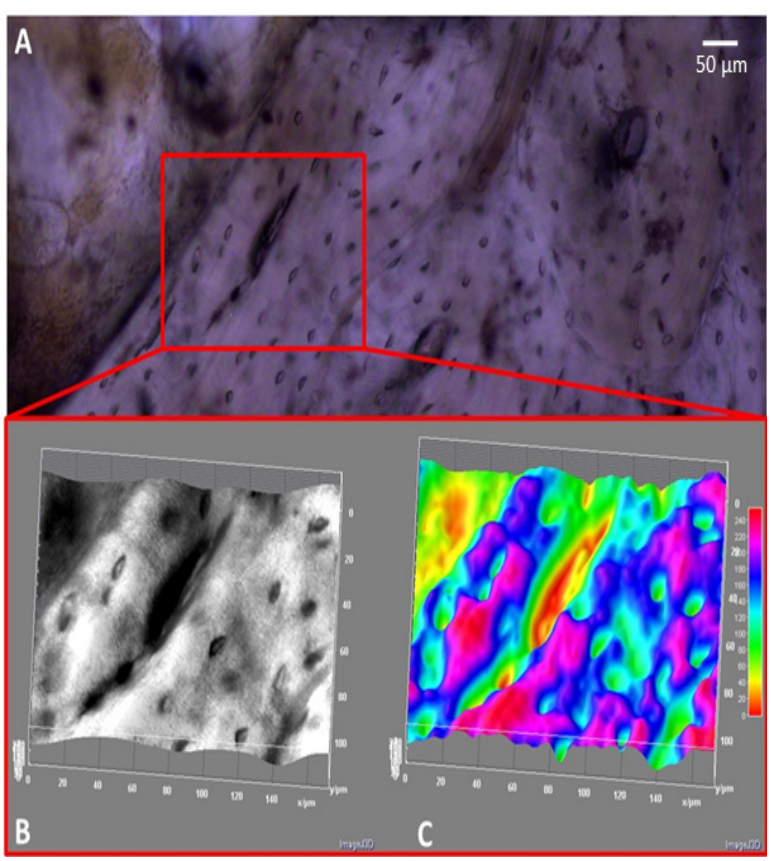

Figure 4. Linear microcrack visualized in 3D. A) Microcrack identified on Polarized light and segmented from the image (red square). B) 3D visualization obtained from A in original collor. C) 3D visualization obtained from A using the Spectrum LUT tool. The microcrack is observed in its deepness in red collor at the center (see histogram scale), surrounded by the borders in yellow. In comparison, visualize the osteocytes lacunae, mostly of them in green, not as deep as the microcrack.

Statistical analysis

Results were expressed as means ± standard deviations and medians. Data were analyzed using GraphPad Prism 5 software (La Jolla, California, USA). Data distribution was assessed by the D'Agostino & Pearson omnibus normality test. With a non-normal distribution of two groups, nonparametric tests were chosen. The difference of microcracks length between cortical and cancellous bone were assessed using Mann-Whitney test. Association was tested with the Chi-square test for microdamage occurrence between the two bone patterns. Spearman's coefficient of correlation was used to identify correlations between speed and bone microdamage. Speed groups comparison was carried out using Kruskal-Wallis test. Results were considered statistically significant when $p \leq 0.05$.

RESULTS

Microscopic analysis revealed cortical bone and its structures, such as Havers channels, osteons of different sizes, and innumerable lacunae of osteocytes included in the matrix. In cancellous bone, trabeculae distributed in their spatial organization were identified, surrounded by medullary spaces filled with medullary tissue. In fluorescence, intense brightness was observed, not only in the bone damage but also on the entire bone surface. In addition, high fluorescent intensity included cancellous and endosteal surfaces, canal surfaces, and all bone chip clusters.

Bone damage was identified in all samples, including all the damage types analyzed, such as: microcracks, diffuse damage, microfractures, and bone chips. Histomorphometry showed that the mean length of microcracks presented both in cancellous (144.9 ± 73.01µm) and cortical bone (121.4 ± 85.10 µm) were not significantly different (p 0.18, table 1).

Table 1. Bone microdamage distribution in cortical and cancellous bone.

Microdamage	Cortical	Cancellous	p
Microcrack length (µm)	121.4 ± 85.10	144.9 ± 73.01	0.18¥
Diffuse damage, n (%)	4 (33)	6 (7)	
Linear microcracks, n (%)	6 (50)	23 (26)	0.0016†*
Microfracture, n (%)	2 (17)	55 (67)	
Total microdamage, n (%)	12 (100)	86 (100)	

Note: ¥Mann-Whitney test. †Chi-square test. *Significant difference ≤ 0.05. n = number.

There was a significant association between the bone damage morphology and bone pattern (p 0.0016), with more microdamage in the cancellous part than in the cortex (table 1). Interestingly, for diffuse damage, the occurrence was one and a half times higher in the cancellous bone than in the cortical bone (table 1). Diffuse damage was quite uncommon compared to linear microcracks. The generation of microcracks was approximately 3.8 times higher in cancellous bone (23 microcracks) than in cortical bone (6 microcracks) (table 1). Regarding microfractures, the occurrence was much higher in the cancellous bone (55 fractures) compared with the cortical bone (2 fractures) (table 1). In relation to the damage analyzed into their depth, 3D visualization of microcracks during confocal microscopic evaluation revealed a wedge format, with the center part being large enough to separate the bone matrix. After the stack creation on the 3D reconstruction, it was possible to identify that one of the microcracks was 35.13 µm in depth and the other was 60.81 µm, on the z axis (meaning depth direction). A plot created with the Spectrum LUT tool was helpful in distinguish the whole microcrack extension and deepness, improving visualization (figure 4).

When comparing bone damage among the three speed groups for the parameters evaluated, no statistical differences concerning bone chip amount, microfracture density, microcrack density, and length (table 2) were observed. In G12, these were more prevalent in the cortical bone (75%, n = 3) than in the cancellous bone (25%, n = 1). On the

contrary, for G8 and G4 these were more common in cancellous bone, with 33.4% (n = 2) in the cortex versus 66.6% (n = 4) in the cancellous bone for G8. No occurrence of diffuse damage was found in cortical bone, and one was found in cancellous bone for G4 (table 2).

In addition, there was a moderate correlation between microfracture density and microdamage density (p 0.05, r' 0.54), revealing that if fracture density increases, microcracks increase too. The other comparisons and correlations were not statistically significant, as follows: Speed – RPM and: a) Fr.D r' 0.08 p 0.76; b) Cr.D r' 0.04 p 0.89; c) Cr.Le r' 0.08, p 0.80.

Table 2. Bone damage comparison among groups and diffuse damage presence.

Parameter	Speed groups			
	G12 (n=12)	G8 (n=11)	G4 (n=9)	p
BC (S)	1.5 ± 0.7 / 1	1.8 ± 1 / 2	1.6 ± 0.7 / 2	0.80
Fr.D (n/mm²)	0.06 ±0.06 / 0.05	0.04± 0.03 / 0.02	0.08 ± 0.11 / 0.04	0.98
Cr.D (n/mm²)	0.03 ± 0.03 / 0.02	0.02 ± 0.03 / 0.0	0.01 ± 0.02 / 0.0	0.41
Cr.Le (µm)	147.6 ± 84.9 / 112	126.1 ± 42.5 / 99	122.2 ± 19.4 / 133	0.86
Diffuse Damage		Groups		
		G12	G8	G4
Cortical bone (n, %)		3 (75)	2 (33.4)	0 (0)
Cancellous bone (n, %)		1 (25)	4 (66.6)	1 (100)
Total		4 (100)	6 (100)	1 (100)

Note: Mean + SD / Median. Kruskal Wallis test. Significant difference ≤.05. BC: bone chips. S: score. Fr.D: microfracture density. Cr.D: microdamage density. Cr.Le: microcrack length.

DISCUSSION

Linear microcracks, diffuse damage, microfractures, and the formation of bone chips were found to be the bone microdamage formed during osteotomy procedure. Both load pressure by drill insertion and the subsequent cutting movements producing vibration were suggested to be related to the different types of microdamage found. These microdamage types were predominantly present in the cancellous bone rather than in the cortex, and this could be explained by both: a) the inherent natural architecture (cancellous bone being less resistant, and tough being the part more prone to reveal the effects of the cutting procedure); b) and by the forces applied in these regions during bone perforation. The differences between cortex and cancellous bone were important to reveal differences in microdamage occurrence after osteotomy. Cortical bone is thicker and presents a typical osteon organization, surrounded by cement lines and interstitial tissue [18,19]. Cancellous bone is characterized by a network of trabeculae whose distribution is organized parallel to the resultant stress lines [20,21]. In our results, the load dissipation during osteotomy revealed more consequences in cancellous bone for microfractures production.

Damage occurred not only in the perforation area, i.e., the borders of the osteotomy, but also in the adjacent bone. Linear microcracks were generated more than diffuse damage, with diffuse damage being quite uncommon in the analyzed histological sections. The most prevalent microdamage in this study was the microfractures for cancellous bone and microcracks for cortical bone. The different drilling rotation speeds had no influence on damage creation or propagation, with a lack of significant differences among the tested groups. However, lower microcrack density was observed in the group with the slowest speed, though with no statistically significant difference.

The use of a bovine bone waste material was considered in this study and was revealed as a good option to assess the mechanical response concerning microdamage generation during turning speed. Anatomy evaluation by visualization reveals a clear definition of cortical and cancellous bone. Also, a variation in the cortical thickness was around 0.5 mm,

which we believe to minimal interference in the results, however, mimicking the physiological condition expected to vary in different sites. Replacement of in vivo study conditions to assess bone behavior in the mechanical analysis was achieved successfully. Besides replacement, the model proposed in this study could be considered an alternative before going on in "in vivo" studies, by testing the mechanical bone material resistance on different protocols. Once tested for microdamage generation, the best osteotomy condition (rotation speed, loading, etc.) could be defined for the in vivo following studies. Frank et al. [22] revealed that experiments have been developed to better understand microdamage formation and how is influenced by material properties. The authors proposed a fatigue test protocol established to induce microdamage in aged and diseased bone, and the evaluation of microdamage at the tissue/material level was presented, which might serve as a basis of microdamage classification at the meso-scale.

Also, interestingly, the results found in this study contribute to a previous discussion about microdamage creation in implant installation. A study reported that the main cause of microcracks creation was the osteotomy preparation before implant placement, and that implant insertion seems to have no major additional effects on damage creation [5]. It was concluded that microdamage may stimulate the remodeling processes, which is important in initial implant integration. However, another study [23] argued that microdamage was induced only by implant insertion and that there was no evidence of microdamage adjacent to the perforations (microcracks, crosshatch, or diffuse damage) in control osteotomy sites. According to our results, the osteotomy drilling procedure was enough to create bone microdamage of 4 different nature and morphology, from small microdamage to microfractures.

Furthermore, an expected correlation between microfracture density and microcracks density was found. It is supposed that damages of distinct morphologies occur simultaneously, which was evidenced by significant correlation of two of them. Osteotomy drilling was enough to produce microcracks, microfractures, and shattering to form the bone chips. Also, the possibility of the influence of a common extraneous factor besides RPM should be considered to understand the simultaneous increase in both fractures and cracks (i.e., drilling trepidation during osteotomy cutting movement, or excessive load applied on the fragment).

Likewise, differences in microdamage morphology are also related to different load applied in tension and compression. Diffuse damage is characterized as compressive damage, and this differs from linear microcracks that are oriented perpendicularly to the tensile stress and characterized as tensile microcracks [7]. In this study, we found both linear microcracks and diffuse damage, although linear microcracks were more present than diffuse damage. Thus, it could be suggested that drilling may be related to proportionally more tensile stress than to compressive stress on the perforation site and adjacent bone. Lower amounts of diffuse damage at the cortex in our samples (only 4) may be related to the inherent characteristics of cutting the bone by using a twist spiral drill, and that the higher amounts of this specific type of damage could appear only after the implant installation. Herman et al. [12], evaluating the bone remodeling process and the differential response to the type of damage at the cortex, revealed that there was no activation of resorption in response to diffuse damage alone. Microcracks and diffuse damage have differential biomechanical responses and outcomes. Diffuse damage is a characteristic of bones that have better fracture resistance, unlike linear microcracks, that may appear at any bone site and that can accumulate and propagate without proper repair [7].

When looking at the different drilling speeds during the osteotomy procedure, we theorize that distinct speeds can generate more or less microdamage. However, we did not find a significant difference between the three speed variations at 1200, 800, and 400 RPM. A limitation of our study was an absence of control group (without any perforation) that shows whether there is physiological microdamage produced in vivo, although once could assume that physiological microcracks would be inconspicuous. Nevertheless, despite the lack of information about the rotation speed interference during osteotomy for implant installation, we believe that this study brings new insights about the subject. To our knowledge, no previous studies have compared different rotation velocities during preparation of the surgical site and its consequences in bone tissues, including damage formation.

CONCLUSION

In conclusion, in vitro drilling osteotomy procedure on a perforation site, simulating a preparation for implant installation, produces bone microdamage resulting in the formation of microcracks, diffuse damage, bone chips, and

microfractures. Not only small linear microdamage was found, but microfractures were present at a reasonable frequency. Cancellous bone was more prone to damage formation rather than the cortex, and linear microcracks appeared more frequently than diffuse damage. Microcracks observed in their depth by 3D visualization revealed the real extension of the damage within the bone. Bone microdamage occurred regardless of the drilling speed. The bovine bone should be considered for ex vivo experiments, for testing drilling and implant installation protocols.

Collaborators

IA Francisquini, conceptualization, methodology, visualization, writing - original draft. GD Rabelo, supervision, methodology, data curation, formal analysis, writing - review & editing. NMSP Assis, supervision, methodology, data curation, writing - review & editing. BS Sotto-Maior: Methodology, data curation, writing - review & editing. PHJO Limirio, methodology, resources. KL Devito, supervision, data curation, writing - review & editing.

REFERENCES

1. Favero V, Sakuma S, Alccayhuaman KAA, Benedetto GA, Bengazi F, Botticelli D. Healing at sites prepared using different drilling protocols. An experimental study in the tibiae of sheep. PLoS One. 2018;13(8):e0202957. http://dx.doi.org/10.1371/journal.pone.0202957
2. Vasilios A, Alevizakos V, Mitov G, Ahrens AM, von See C. The influence of implant site preparation and sterilization on the performance and wear of implant drills. Int J Oral Maxillofac Implants. 2021;36(3):546-552. http://dx.doi.org/10.11607/jomi.8099
3. Ercoli C, Funkenbusch PD, Lee H-J, Moss ME, Graser GN. The influence of drill wear on cutting efficiency and heat production during osteotomy preparation for dental implants: a study of drill durability. Int J Oral Maxillofac Implants. 2004;19(3):335-49.
4. Ponzoni D, Martins FEPB, Conforte JJ, Egas LS, Tonini KR, de Carvalho PSP. Evaluation of immediate cell viability and repair of osteotomies for implants using drills and piezosurgery. A randomized, prospective, and controlled rabbit study. Clin Implant Dent Relat Res. 2020; 22(3):250-260. http://dx.doi.org/10.1111/cid.12907
5. Warreth A, Polyzois I, Lee CT, Claffey N. Generation of microdamage around endosseous implants. Clin Oral Implants Res. 2009;20(12):1300-6. http://dx.doi.org/10.1111/j.1600-0501.2009.01808.x.
6. Huja SS, Katona TR, Burr DB, Garetto LP, Roberts WE. Microdamage adjacent to endosseous implants. Bone. 1999;25(2):217-22. http://dx.doi.org/10.1016/s8756-3282(99)00151-9
7. Dominguez VM, Agnew AM. Microdamage as a bone quality component: practical guidelines for the two-dimensional analysis of linear microcracks in human cortical bone. JBMR Plus. 2019; 3(6):e10203. http://dx.doi.org/10.1002/jbm4.10203
8. Kennedy OD, Lendhey M, Mauer P, Philip A, Basta-Pljakic J, Schaffler MB. Microdamage induced by in vivo reference point indentation in mice is repaired by osteocyte-apoptosis mediated remodeling. Bone. 2017; 95:192-198. http://dx.doi.org/10.1016/j.bone.2016.11.029
9. Wu LJ, Hsieh KH, Lin CL. Integrating finite element death technique and bone remodeling theory to predict screw loosening affected by radiation treatment after mandibular reconstruction surgery. Diagnostics (Basel). 2020;10(10):844. http://dx.doi.org/10.3390/diagnostics10100844
10. Wolfram U, Schwiedrzik JJ, Mirzaali MJ, Bürki A, Varga P, Olivier C, et al. Characterizing microcrack orientation distribution functions in osteonal bone samples. J Microsc. 2016; 264(3):268-281. http://dx.doi.org/10.1111/jmi.12440
11. Liu X, Tang C, Zhang X, Cai J, Yan Z, Xie K, et al. Spatiotemporal distribution of linear microcracks and diffuse microdamage following daily bouts of fatigue loading of rat ulnae. J Orthop Res. 2019; 37(10):2112-2121. doi: 10.1002/jor.24391.
12. Herman BC, Cardoso L, Majeska RJ, Jepsen KJ, Schaffler MB. Activation of bone remodeling after fatigue: Differential response to linear microcracks and diffuse damage. Bone. 2010;47(4):766-72. http://dx.doi.org/10.1016/j.bone.2010.07.006
13. Lowe T, Avcu E, Bousser E, Sellers W, Withers PJ. 3D Imaging of indentation damage in bone. Materials. 2018; 11(12):2533. http://dx.doi.org/10.3390/ma11122533
14. Huiyu H, Chengyong W, Yue Z, Yanbin Z, Linlin X, Guoneng X, et al. Investigating bone chip formation in craniotomy. Proc Inst Mech Eng Part H J Eng Med. 2017;231(10):959-74. http://dx.doi.org/10.1177/0954411917727245
15. Misir AF, Sumer M, Yenisey M, Ergioglu E. Effect of surgical drill guide on heat generated from implant drilling. J Oral Maxillofac Surg. 2009;67(12):2663-8. http://dx.doi.org/10.1016/j.joms.2009.07.056
16. Sumer M, Misir AF, Telcioglu NT, Ahmet UG, Yenisey M. Comparison of heat generation during implant drilling using stainless steel and ceramic drills. J Oral Maxillofac Surg. 2011;69(5):1350-4. http://dx.doi.org/10.1016/j.joms.2010.11.001
17. Francisquini IA, Caldas RA, Rabelo GD. Bone microdamage evaluation: a supplementary tool to provide three-dimensional visualization. Clin Lab Res Den. 2020;1-7. http://dx.doi.org/10.11606/issn.2357-8041.clrd.2020.170117

18. Farlay D, Boivin G. Bone mineral quality. Osteoporosis. 2012;953-78.

19. Liu Y, Chen B, Yin D. Effects of direction and shape of osteocyte lacunae on resisting impact and micro-damage of osteon. J Mater Sci Mater Med. 2017;8(3):38. http://dx.doi.org/10.1007/s10856-017-5850-6

20. Chappard Chappard D, Baslé MF, Legrand E, Audran M. Trabecular bone microarchitecture: a review. Morphologie. 2008;92(299):162-70. http://dx.doi.org/10.1016/j.morpho.2008.10.003

21. Buccino F, Colombo C, Vergani LM. A review on multiscale bone damage: from the clinical to the research perspective. Materials (Basel). 2021;14(5):1240. http://dx.doi.org/10.3390/ma14051240

22. Frank M, Fischer JT, Thurner PJ. Microdamage formation in individual bovine trabeculae during fatigue testing. J Biomech. 2021;115:110-31. http://dx.doi.org/10.1016/j.jbiomech.2020.110131

23. Raghavendra S, Wood MC, Taylor TD. Early wound healing around endosseous implants: a review of the literature. Int J Oral Maxillofac Implants. 2005; 20(3):425-31.

Received on: 18/8/2020
Approved on: 25/1/2022

Assistant editor: Fabiana Mantovani Gomes França